IMPROVEMENT OF THE HEAT EXCHANGE CHARACTERISTICS OF PARALLEL CORRUGATED FINNED TUBES BY PERFORATION

by
Jinxing WU*, Tianwei GU, Shiwu HOU, Jiahui YI, and Peng SHAO
School of Mechanical and Power Engineering, Zhengzhou University, Zhengzhou, China

Original scientific paper
https://doi.org/10.2298/TSCI251029020W

To further enhance the heat exchange performance of parallel corrugated fins (PCF), this study proposes perforation on PCF and comparison and analyze the velocity and temperature fields of PCF and perforated PCF (PPCF). It was found that perforation can reduce the thickness of the temperature boundary-layer, thereby enhance the convective heat transfer efficiency. Under the operating conditions where Reynolds number is 9000-21000, the influence laws of the perforation position parameter, Sl, on the heat exchange performance were studied. The numerical simulation results show that when Sl = 5/4, the heat transfer enhancement effect of the perforated structure is the best. Based on the field synergy theory, the enhanced heat transfer mechanism of PPCF was analyzed. This research provides a new solution for the structural improvement of PCF.

Keywords: *corrugated finned tube, heat exchanger, perforated fin, heat transfer enhancement, numerical simulation*

Introduction

Finned tube heat exchangers have the advantages of high heat transfer efficiency, good compact structure and long service life, and are widely used in industrial fields such as vehicle air conditioning, building air conditioning, and battery cooling. The basic component of a finned tube heat exchanger is the finned tube, with gas outside the tube. The heat inside the tube is transferred to the fins outside through heat conduction. Gas-flows through the finned tube and exchanges heat via convection. This achieves heat exchange between cold and hot fluids. The thermal resistance in the heat transfer process is mainly concentrated on the air side. Therefore, optimizing the air-side heat transfer structure to enhance exchanger performance is very common [1-3].

The corrugated surface increases the air-fin contact area. It also significantly disturbs the fluid [4-8], leading to better heat exchange performance. This has attracted much research interest. Most of the early research was carried out in experimental form. Kang *et al.* [9] experimentally studied the air-side heat transfer and resistance characteristics of 12 three-row shell-and-tube heat exchangers with four fin structures. Within the measured Reynolds number range, the Nusselt number on the surface of the Slit fin is the largest. Wang *et al.* [10, 11] found

*Corresponding author, e-mail: 15890918454@163.com

that the enhanced heat transfer effect of corrugated fins was only significant when the fin spacing was small and the ripple height was large. Notably, this structure caused considerable pressure loss throughout the experiment. Youn and Kim [12] studied finned tube heat exchangers with different corrugation shapes. The results showed that while sinusoidal corrugated finned tubes brought better heat transfer effects, they also had greater pressure losses.

Many geometric parameters affect corrugated finned tube heat exchangers. Therefore, pure experimental research consumes significant cost and effort, while numerical simulation research greatly reduces the cost of such research. Sadeghianjahromi *et al.* [13] investigated how different schemes affect finned tube heat exchanger performance. They found that combining increased corrugation height, added vortex generators (VG) and slit manufacturing yields the most significant thermal resistance reduction. Ouyang *et al.* [14] conducted numerical simulations on the interlaced and parallel arranged corrugated finned tubes. The results show that the interlaced corrugated arrangement has a better heat transfer effect than the parallel corrugated arrangement. Under laminar flow conditions, Song *et al*. [15] studied concave and convex triangular fins in plate air cooler channels. They found concave arc-shaped fins enhance heat transfer, while convex ones weaken it.

In the field of heat exchanger research, enhancing heat transfer efficiency has always been a key focus. Passive heat transfer enhancement technology is widely used in various heat exchangers. For instance, in the enhanced heat transfer of finned tube heat exchangers, common means of enhanced heat transfer include the use of VG and slit perforation, *etc*. Kataoka *et al.* [16] believes that VG reduces the thickness of the boundary-layer, thereby improving heat exchange. Johnson and Joubert [17] were the first to publish a research paper on VG. They studied how vortices from these devices affect cylinder heat transfer and pressure drop, and found a synchronous effect: higher heat transfer capacity coincides with increased pressure drop. Wang *et al.* [18] found through numerical methods that the triangular wing vortex generator (VG-D) achieved effective mixing of cold and hot fluids by generating longitudinal vortices. The heat exchange capacity of the fin surface has thus been enhanced.

Liu *et al.*[19] enhanced heat transfer by adding slit perforations on the windproof side of wavy fins, resulting in a 5.5% improvement in thermal performance. Su *et al.* [20] studied four different types of slit fins under laminar flow conditions, all of which demonstrated superior heat transfer efficiency compared to traditional fins. Karabacak and Yakar [21] experimentally investigated the influence of perforated finned tubes on heat transfer and convection. The results indicated that the heat transfer of the perforated finned heater was 12% higher than that of the non-perforated finned heater. Song *et al.* [22] numerically investigated the influence of perforations of different diameters on helical fins on flow and heat transfer. They found that the perforations caused jet impacts in the fluid, generating strong turbulent kinetic energy in the helical channel. Zaidan *et al.* [23] numerically simulated the heat transfer and flow characteristics of air on flat finned tubes with circular, square and triangular perforated fins, and found that the triangular perforation had the most significant effect on improving the performance of the heat exchanger.

Based on the previous research, it can be found that the corrugated design disrupts the boundary-layer, promotes turbulent mixing, and increases the heat exchange rate between the fluid and the fin surface. Moreover, perforation in the fins can also effectively enhance the heat exchange performance. Due to the prominent axial velocity of gas in the alternating up-and-down flow between corrugated fins (compared to straight or spiral fins), perforations are speculated to significantly affect flow fields and heat transfer, an underexplored gap that aligns with our team's long-term focus on structural optimization for heat transfer enhancement.

Our team has achieved notable research results in enhancing heat transfer through structural optimization in the past: when the helix angle of the helical finned tube is less than 25°, the comprehensive performance continuously improves [24, 25]; the helical rod enhances the comprehensive heat transfer performance by more than 10.8% [26]. After adding grooves to the helical tube, the performance evaluation criterion (PEC) can be increased by up to 59.33% [27]. Building on this foundation of structural optimization for heat transfer enhancement, this study shifts focus to PCF, a structure not explored in our previous work. We analyze the enhanced heat transfer mechanism of perforations by means of the field synergy principle and define the dimensionless perforation position parameter, *Sl*, for the first time to quantify the influence of the relative position of perforations on heat transfer performance.

Table 1 shows the advantages and disadvantages of some existing finned tube improvement schemes compared with PPCF. Compared with other schemes, PPCF has considerable advantages in heat transfer and overall performance, and its structural design is simple, processing cost is controllable, and it has stronger engineering applicability. However, it should be noted that the resistance loss of PPCF is relatively large, which becomes the main constraint on its performance improvement. The research results of this paper are expected to provide important technical references and theoretical support for the design of finned tube heat exchangers with superior performance.

Table 1. The comparison between PPCF and other improvement schemes

Case	Improvement plan for finned tubes	Advantage	Disadvantage
1	Compound-structured wavy finned tube [13]	High comprehensive performance	Ordinary heat transfer performance, high processing difficulty
2	Staggered corrugated finned tubes [14]	Excellent heat transfer performance	Large pressure drop
3	Annular elliptical finned tube [6]	Significant reduction in pressure loss.	Poor heat transfer performance
4	PPCF tube	Significant advantage in heat transfer performance; comprehensive performance higher than Case 2	Large pressure drop

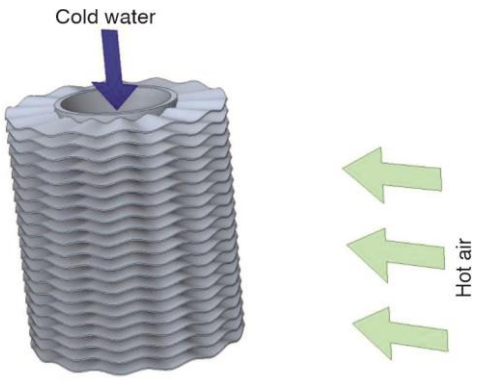

Figure 1. Geometric model of heat exchanger with parallel corrugated finned tubes

Details of numerical information

Mathematical representation

To illustrate the working principle of finned tubes, a structural schematic of the finned tube heat exchanger is presented in fig. 1. Hot fluid flows outside the tubes, and cold fluid inside, with heat exchange occurring via the tube walls and fins.

In this study, FLUENT 2022R1 was used for simulations. The finite volume method was adopted to discretize the governing equations, and the SIMPLE algorithm was employed to couple the pressure and velocity fields under

steady-state conditions. Air is treated as an incompressible fluid with constant physical properties to simulate the flow and heat transfer in the fluid domain, and its thermophysical properties are listed in tab. 2.

Table 2. Property parameters of air

Parameter	ρ [kgm^{-3}]	c_p [Jkg^{-1}K^{-1}]	λ [Wm^{-1}K^{-1}]	$\mu \times 10^5$ [Pa·s]
Value	1.225	1006.43	0.0242	1.7894

The Reynolds number range is defined as 9000-21000, which highlights the advantages of perforation while preventing excessive energy consumption caused by high Reynolds number values, thus enhancing its engineering value. Numerical simulation was carried out using the SST k-ω turbulence model. The governing equations without considering radiation, viscous dissipation and gravity are.

Continuity equation:

$$\frac{\partial}{\partial x_i}\rho u_i = 0 \tag{1}$$

The momentum equation of turbulence:

$$\frac{\partial}{\partial x_i}\left(\rho u_i u_j\right) = -\frac{\partial p}{\partial x_j} + \frac{\partial}{\partial x_i}\left[\left(\mu + \mu_t\right)\frac{\partial u_j}{\partial x_i}\right] \tag{2}$$

Energy equation of turbulence in the fluid region:

$$\frac{\partial}{\partial x_i}\left(\rho c_p u_i T\right) = \frac{\partial}{\partial x_i}\left[\left(\lambda + \lambda_t\right)\frac{\partial T}{\partial x_i}\right] \tag{3}$$

k and ω:

$$\frac{\partial}{\partial x_i}\left(\rho k u_i\right) = \frac{\partial}{\partial x_i}\left[\left(\mu + \mu_t\right)\frac{\partial k}{\partial x_i}\right] + G_k - \beta^* \rho\omega k \tag{4}$$

$$\frac{\partial}{\partial x_i}\left(\rho k u_i\right) = \frac{\partial}{\partial x_i}\left[\left(\mu + \mu_t\right)\frac{\partial \omega}{\partial x_i}\right] + \alpha\frac{\omega}{k}G_k - \beta\rho\omega^2 \tag{5}$$

where $\mu_t = \rho k/\omega$, $\alpha = 0.52$, $\beta^* = 0.09$, and $\beta = 0.072$.

In the previous equations, μ is the dynamic viscosity, μ_t – the turbulent viscosity, ρ – the density, λ – the thermal conductivity, c_p – the specific heat capacity, λ_t – the turbulent thermal conductivity, and G_k – the turbulence kinetic energy of the fluid.

Computational domain and boundary conditions

The boundary conditions and corresponding values are listed in tab. 3. Too low a wall temperature enlarges the temperature difference between the wall and the working medium, causing a significant deviation from the incompressibility assumption and thus undermining the simulation model's reliability. Conversely, an overly high wall temperature weakens the heat transfer driving force, making it difficult to demonstrate the advantages of the perforated structure. Considering these aspects, the wall temperature is set to 273 K.

Figure 2(a) presents a schematic of the PPCF physical model. The finned tube design complies with China's national mechanical industry recommended standard: *Finned Heat Exchangers for Freon Refrigeration Devices* (JB/T 7659.5-1995). To ensure uniform air-flow di-

Table 3. Boundary condition in simulation

Boundary name	Boundary conditions and descriptions	Value
Inlet	Velocity inlet	1.26, 1.68, 2.1, 2.52, 2.94 m/s; 300 K
Outlet	Pressure outlet	0 Pa
Symmetry	Symmetry	–
Periodic	Periodic	–
Heat wall	Constant wall temperature; non-slip wall	273 K

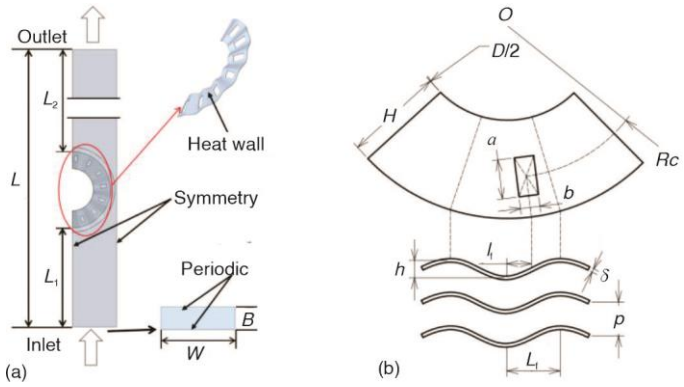

Figure 2. Geometric model diagram;
(a) overall geometric model diagram and (b) fin size diagram

stribution, the inlet computational section is extended to >1.5 times the finned tube hydraulic diameter. Similarly, the outlet section is lengthened to >5 times the hydraulic diameter to eliminate backflow [3]. The geometric parameters are summarized in tab. 4.

Table 4. Geometric parameters

Geometric parameters	L	L_1	L_2	W	B	Rc	H	h
Value [mm]	500	87.6	338	41	12.48	28.7	15.7	1.6
Geometric parameters	D	a	b	δ	l_f	L_f	p	
Value [mm]	39	7.47	3.735	0.19	3.195	6.39	1.58	

Heat exchanger performance

The heat transfer rate, Q, and the heat transfer coefficient, h_0, are calculated:

$$Q = c_p \dot{m} \Delta t \tag{6}$$

$$h_0 = \frac{Q}{A_w \Delta T} \tag{7}$$

where $\dot{m}$ is the mass-flow rate of air, Δt – the temperature difference between the air inlet and outlet, A_w – the outer surface area of the base tube, and ΔT – the logarithmic mean temperature difference. The calculation method is shown in:

$$\Delta T = \frac{\left(t_w - t_{in}\right) - \left(t_w - t_{out}\right)}{\ln\left[\dfrac{\left(t_w - t_{in}\right)}{\left(t_w - t_{out}\right)}\right]} \tag{8}$$

where t_w is the wall temperature of the heat exchanger tubes.

Reynolds number calculation formula:

$$\mathrm{Re} = \frac{\rho v_{\max} D_h}{\mu} \tag{9}$$

where D_h is the hydraulic diameter, equivalent to the outer diameter of the finned tube and v_{max} – the air velocity at the narrowest section, and its calculation is given by the following equation:

$$v_{\max} = v_{in} \frac{BW}{A_{\min}} \tag{10}$$

where A_{min} is the minimum cross-sectional area. The Nusselt number and friction factor, f, are calculated using:

$$\mathrm{Nu} = \frac{h_0 D_h}{\lambda} \tag{11}$$

$$f = \frac{2\Delta p}{\rho v_{\max}^2} \frac{D_h}{L} \tag{12}$$

where λ is the fluid thermal conductivity, Δp – the pressure difference at the inlet and outlet of the fluid, L – the flow channel length, and v_{max} – the average velocity through the minimum cross-sectional area. For passive heat transfer enhancement techniques in heat exchangers, improved heat transfer performance is invariably accompanied by increased pressure loss. To balance these two competing effects, the PEC is employed to assess the heat exchanger's overall thermal performance. The formula is:

$$PEC = \frac{\dfrac{\mathrm{Nu}}{\mathrm{Nu}_0}}{\left(\dfrac{f}{f_0}\right)^{1/3}} \tag{13}$$

where the subscript 0 denotes the parameter values for PCF.

Guo *et al.* [28] re-examined the physical mechanism of convective heat transfer based on the co-ordination between the velocity and temperature field, and proposed the field synergy theory for heat transfer enhancement. According to this theory, a larger cosine value of the angle between the velocity vector and temperature gradient vector (*i.e.*, a smaller synergy angle β) corresponds to stronger synergy between the velocity and temperature gradient fields, thereby yielding superior convective heat transfer performance. The formula for calculating the field synergy angle β is given as:

$$\beta = \arccos \frac{U \times \Delta T}{|U| \times |\Delta T|} \tag{14}$$

Numerical methods and grid independence

In this work, unstructured polyhedral meshes were generated using FLUENT MESHING. To resolve the local physical quantity distributions near the tube outer wall and fin surfaces, a 10 layer boundary-layer was constructed with a first-layer height of 0.025 mm and a growth rate of 1.0. Grid generation details are shown in fig. 3. A grid independence study was

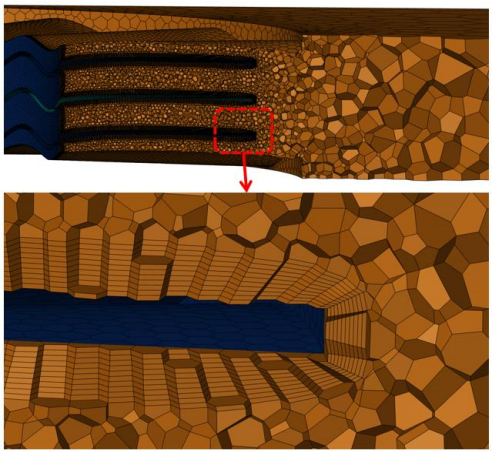

Figure 3. Details of grid division

performed using the heat exchanger's pressure drop and heat transfer coefficient as evaluation metrics, with their relationship to grid number illustrated in fig. 4(a). Beyond the fourth grid set, the heat transfer coefficient stabilizes with a relative variation below 0.5%. Considering computational efficiency and accuracy, all subsequent simulations adopt the grid size specifications of this set. For this grid configuration, the maximum local wall curvature size is 0.3 mm, a parameter that remains constant in subsequent investigations. To compare the calculation results with the experimental results, the same conditions proposed by FaJiang *et al.* [29] are adopted in this model. The comparison results are shown in fig. 4(b). The verification metrics include the Nusselt number and Euler number derived from both numerical simulations and experimental results. The maximum discrepancies between the simulated and experimental values of these two parameters are 3.31% and 4.9%, respectively. Given the good agreement between the numerical and experimental data, this model is validated for the calculations in the present study.

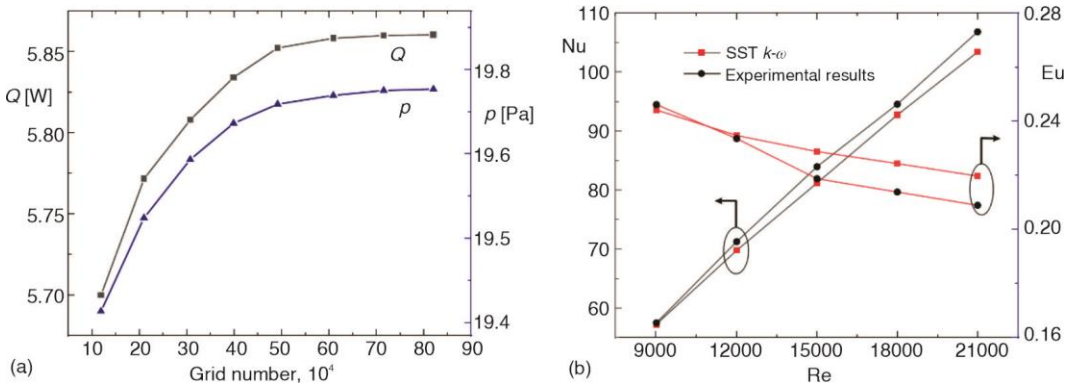

Figure 4. Grid independence testing and model verification; (a) grid independence and (b) model verification

Result discussion

The influence of perforation on the performance of finned tubes

Figure 5 illustrates the variation trends of Nusselt number, *f*, and PEC with the Reynolds number for PPCF and baseline PCF. For both configurations, Nusselt number increases with rising Reynolds number, whereas *f* exhibits a decreasing trend. Compared to the PCF, the PPCF yields higher Nusselt number and *f* with maximum increments of 19.55% and 16.92%, respectively. This indicates that the PPCF enhances the heat exchange effect at the cost of increasing resistance loss. Furthermore, the PPCF achieves a PEC value up to 1.13 times that of the PCF, confirming a substantial improvement in the overall heat transfer performance.

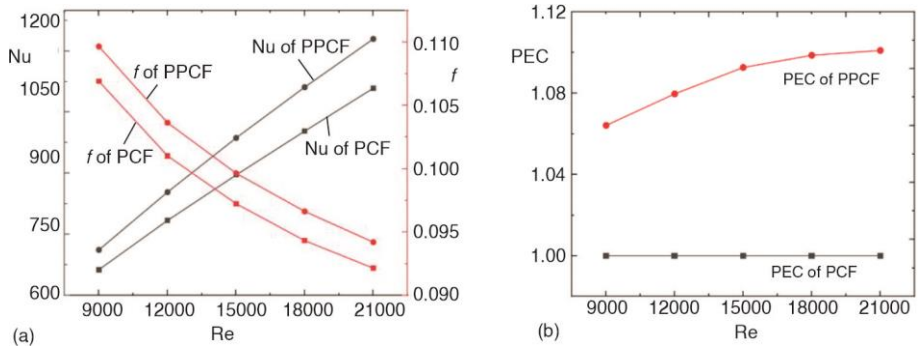

Figure 5. Comparison of *Nusselt number*, *f*, and PEC before and after perforation; (a) comparison of Nusselt number and *f* before and after perforation and (b) comparison of PEC before and after perforation

To streamline the analysis, the heat transfer enhancement mechanism of the PPCF was investigated using data at Re = 21000, where the structure's performance advantages are most pronounced. The selected profile plane-A is positioned at $X = -26.5$ mm (with the base tube center at the coordinate origin). As shown in fig. 6 is the position of plane-A.

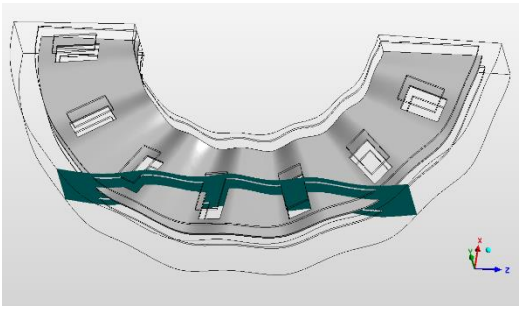

Figure 6. The position of plane-A

Figure 7 presents the velocity field and velocity vector plots at plane-A for Re = 21000. As observed from the plots, the PCF

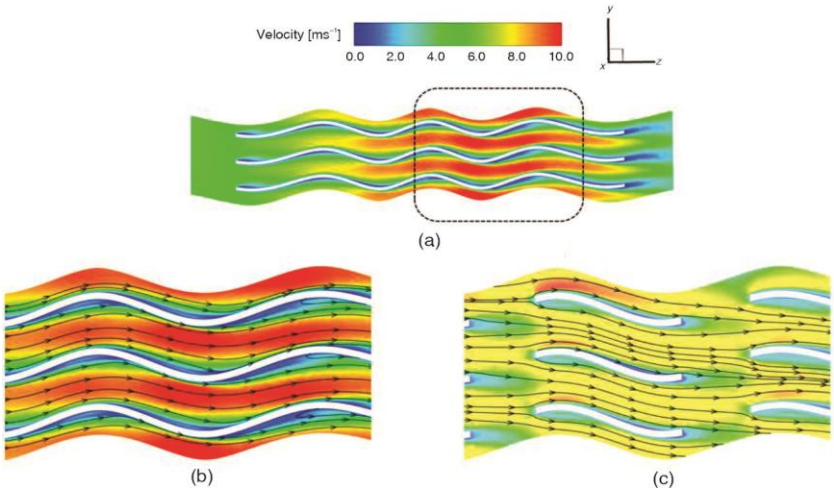

Figure 7. The velocity field and velocity vector diagram at plane-A when Re = 21000; (a) PCF velocity field, (b) PCF local vector diagram, and (c) PPCF local vector diagram

is prone to boundary-layer separation on the leeward side, causing a sudden drop in fluid flow velocity and creating low-speed or even stagnant *dead zones*. In these regions, the relative

motion between the fluid and fin surfaces is suppressed; heat transfer is thus dominated by pure thermal conduction, which substantially degrades the local heat transfer effectiveness.

The PPCF allows some high-speed fluids in the main flow area to directly seep into the low-speed area on the leeward side through the channels, impacting and disturbing the stagnant fluid. This process forces the dead zone fluid to re-participate in the flow, significantly reducing the low-speed area and homogenizing the velocity distribution between the fins, thereby enhancing the overall heat transfer efficiency.

Figure 8 illustrates the distribution of field synergy coefficient for the PCF and PPCF at plane-A. A comparison of the field synergy angles for these two configurations reveals that the PPCF yields a smaller synergy angle, particularly within the flow diversion regions downstream of the perforations. The flow diversion of the fluid through the perforation causes disturbance to the fluid in the adjacent layer, intensifying inter-fluid mixing, reducing the field synergy angle between the velocity and temperature fields, and enhancing the overall heat transfer performance.

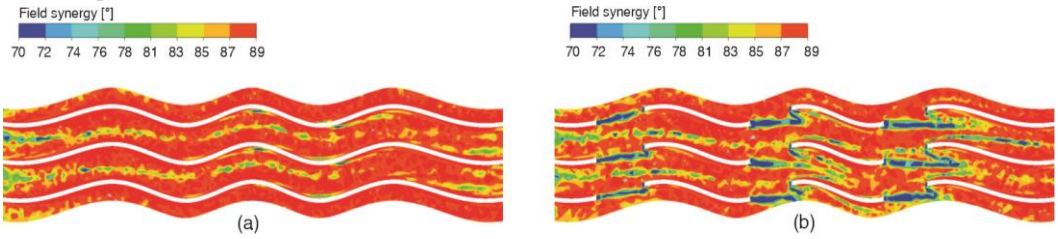

Figure 8. The distribution of field synergies of different structures at Re = 21000; (a) PCF and (b) PPCF

The influence of perforation parameters on the performance of heat exchangers

The geometric parameters of PPCF have a significant impact on the inter-fin flow characteristics. To optimize its heat transfer performance, an investigation into the PPCF with different perforation configurations is thus warranted. This section focuses on the influence of the perforation position parameter, *Sl* ($Sl = l_f/L_f$) on the thermal performance of the PPCF.

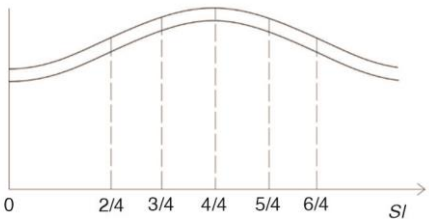

Figure 9. Schematic diagram of *Sl*

To make the research more universal, a dimensionless position parameter, *Sl,* is defined to describe the relative position of the perforation on the corrugated fin. Specifically, the ratio of l_f to L_f, *Sl* = 2/4, 3/4, 4/4, 5/4, 6/4. The schematic diagrams of different *Sl* are presented in fig. 9.

Figure 10 presents the local velocity vector plots and pressure contour plots for plane A. In fig. 10(c), at the perforation position of *Sl* = 3/4, a small amount of fluid undergoes diversion through the perforation, and the impact on the performance of the heat exchanger is also minimal. From the velocity vector diagram in fig. 10(a), at the position *Sl* = 3/4, the fluid flow direction near the fin is roughly parallel to the fin surface. After perforation, the fluid still flows parallel to the fin surface, resulting in negligible flow diversion at this perforation location. In addition, perforation causes the fin structure to be discontinuous, resulting in intense separation and reattachment of the boundary-layer, which in turn significantly enhances the

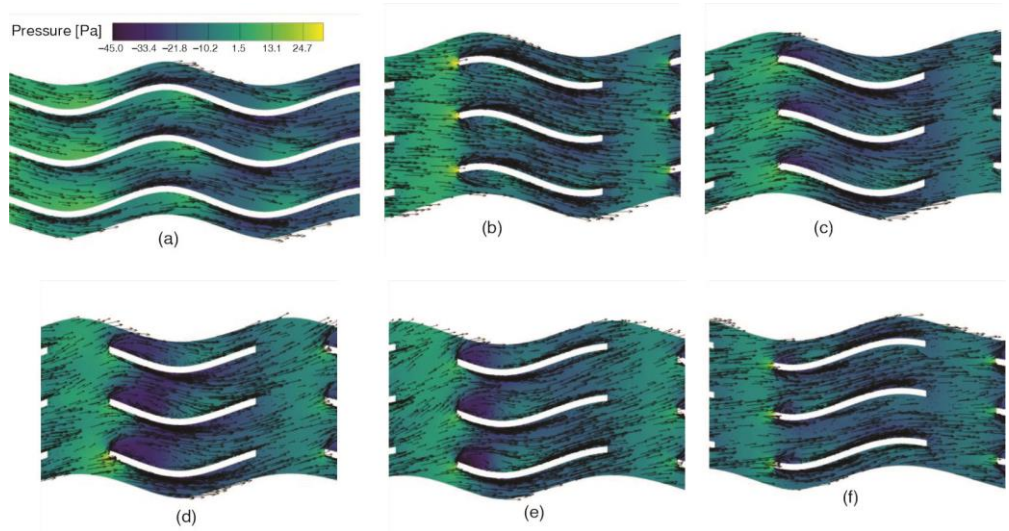

Figure 10. Local velocity vector diagram and pressure cloud diagram of section A; (a) PCF, (b) *Sl* = 2/4, (c) *Sl* = 3/4, (d) *Sl* = 4/4, (e) *Sl* = 5/4, and (f) *Sl* = 6/4

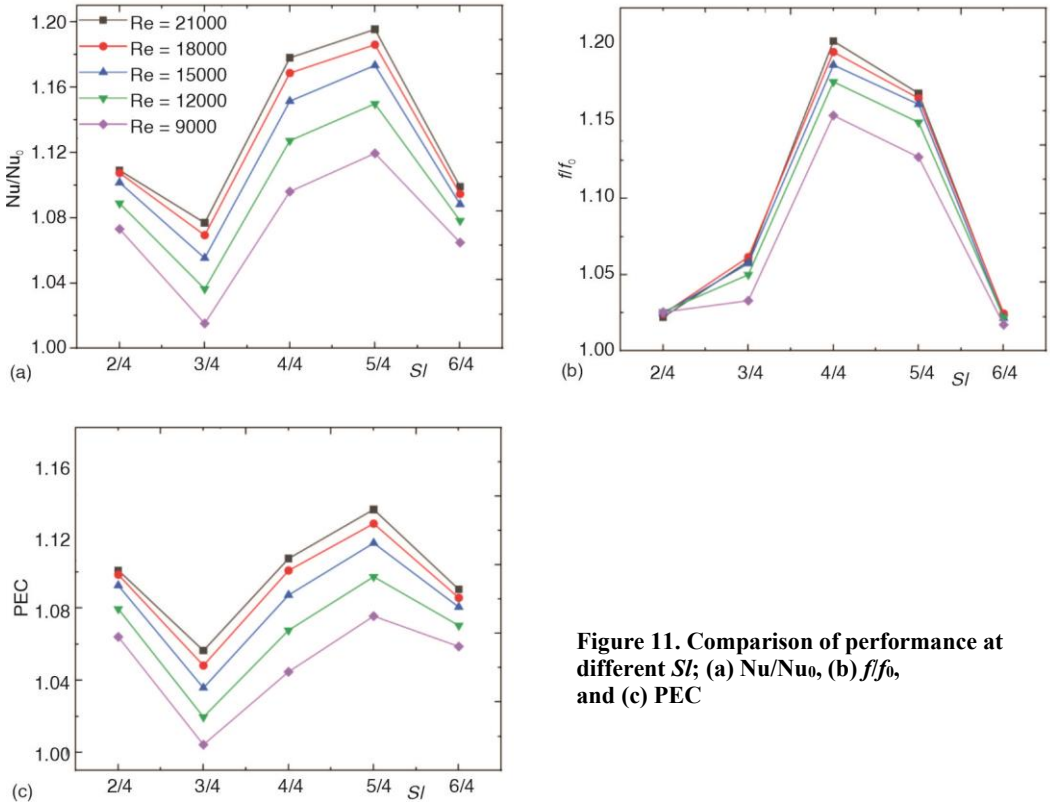

Figure 11. Comparison of performance at different *Sl*; (a) Nu/Nu_0, (b) f/f_0, and (c) PEC

intensity of convective heat transfer. Meanwhile, the elevated fluid flow resistance directly gives rise to a higher pressure drop. Correspondingly, as observed in figs. 10(b), 10(d), 10(e),

and 10(f), the perforation-induced flow diversion effect becomes increasingly pronounced under the combined action of inertial force and pressure difference. As analyzed in 3.1, this flow diversion effectively facilitates fluid mixing and intensifies flow perturbations, thereby augmenting convective heat transfer.

Notably, the perforated fin configuration with Sl = 4/4 cause more obvious flow separation of the fluid, resulting in a larger negative pressure zone on the leeward side of the fins. The enhancement of the negative pressure zone will intensify the shear effect between fluids, leading to increased energy dissipation and thus a substantial rise in flow pressure drop.

Figure 11 shows the variations of Nu/Nu_0, f/f_0, and PEC of finned tubes with different perforation positions with Reynolds numbers. As observed from the plots, the Nu/Nu_0 and f/f_0 values for all perforated finned tube configurations with different Sl increase with rising Reynolds numbers.

When Reynolds numbers is within the range of 9000 to 21000, the variation curves of Nu/Nu_0 and PEC approximate an inverted "N" shape as Sl increases. They first decrease at Sl = 3/4, then increase, and continue to decrease after Sl = 5/4. The changing trend of f is to increase first and then decrease. The thermal performance enhancement is minimal at Sl = 3/4 position, where the corresponding PEC value also reaches its minimum. For varying Sl values and at the same Reynolds number, the Nusselt number of the PPCF exhibits an increase of 1.53%-19.55% relative to the baseline PCF, with the friction factor, f, showing a corresponding increase of 1.73%-20.34%. Specifically, the PPCF attains its maximum PEC at Sl = 5/4, at this optimal configuration, the Nusselt number is elevated by 11.95%-19.55%, the f by 12.73%-16.92%, and the PEC by 7.57%-13.48% compared with the PCF.

Conclusions

In this paper, numerical studies were conducted on the thermal performance of perforated parallel corrugated finned tubes under different working conditions. The enhanced heat transfer mechanism was analyzed. The main conclusions are as follows.

- The perforation design induces the fluid to penetrate laterally through the fin surface of the PCF, enhances the synergy between the fluid velocity vector and temperature gradient in the inter-fin space, and thus augments the overall thermal-hydraulic performance. Compared with PCF, PPCF can increase Nusselt number by up to 19.55%, f by 16.92%, and PEC by 13.48%.
- The perforation position has a significant impact on the thermal performance of PPCF. As the perforation position parameter, Sl, increases, the thermal performance curve for the PPCF approximates a mirror-inverted “N” shape. The PPCF achieves optimal thermal-hydraulic performance at Sl = 5/4.

Nomenclature

A – area, [m^2]
a – length of perforation, [mm]
B – entrance height, [mm]
b – width of perforation, [mm]
c_p – heat capacity at constant pressure, [Jkg^{-1}K^{-1}]
D – outer diameter of tube, [mm]
f –friction coefficient, [–]
G_k – kinetic energy of turbulence, [m^{2}s^{-2}]
H – fin height, [mm]
h – wave height, [mm]
h_0 – heat transfer coefficient, [Wm^{-2}K^{-1}]
L – length of the flow channel, [mm]
L_1 – length of the entrance section, [mm]
L_2 – length of the exit section, [mm]
L_f – distance between a wave crest and the adjacent wave trough, [mm]
l_f – distance from the center of the perforation to the previous wave trough, [mm]
$\dot{m}$ – mass flow rate of air, [kgs^{-1}]
Nu – Nusselt number, [–]
p – fin pitch, [mm]

Q – heat transfer rate, [W]
Re – Reynolds number, [–]
Sl – perforation position parameter
ΔT – logarithmic mean temperature difference [K]
Δt – temperature difference between the air inlet and outlet, [K]
u – velocity, [ms^{-1}]
W – entrance width, [mm]

Grek symbols

β – field synergy angle, [°]
δ – fin thickness, [mm]
λ – thermal conductivity, [Wm^{-1}K^{-1}]
λt – turbulent thermal conductivity,[Wm^{-1}K^{-1}]
μ – dynamic viscosity, [Pa·s]
μt – turbulent viscosity, [Pa·s]
ρ – density, [kgm^{-3}]

Subscripts

h – hydraulic
in – inlet
max – maximum
min – minimum
out – outlet
w – heat wall
0 – parallel corrugated fins

Acronyms

PEC – performance evaluation criterion
PCF – parallel corrugated fins
PPCF – perforated parallel corrugated fins
VG – vortex generator

References

[1] Li, X. Y., *et al.*, Experimental Study on Heat Transfer and Pressure Drop Characteristics of Fin-and-Tube Surface with Four Convex-Strips Around Each Tube, *International Journal of Heat and Mass Transfer, 116* (2018), Jan., pp. 1085-1095
[2] Li, X. Y., *et al*., Numerical Study on the Heat Transfer and Pressure Drop Characteristics of Fin-and-Tube Surface with Four Round-Convex Strips Around Each Tube, *International Journal of Heat and Mass Transfer, 158* (2020), 120034
[3] Wang, Z., Ouyang, X., Numerical Simulation of Heat Transfer and Flow Characteristics for Plate Fin-and-Tube Heat Exchanger with Ring-Bridge Slit Fins, *Thermal Science, 25* (2023), 1A, pp. 77-88
[4] Nemati, H., *et al*., Shape Optimisation of Air-Cooled Finned-Tube Heat Exchangers, *International Journal of Thermal Sciences, 150* (2020), 106233
[5] Nemati, H., *et al*., Natural Convection Heat Transfer Over Horizontal Annular Elliptical Finned Tubes, *International Communications in Heat and Mass Transfer, 118* (2020), 104823
[6] Nemati, H., Samivand S., Numerical Study of Flow Over Annular Elliptical Finned Tube Heat Exchangers, *Arabian Journal for Science and Engineering, 41* (2016), June, pp. 4625-4634
[7] Zhang, D., *et al*., Mathematical Investigation of Heat Transfer Characteristics and Parameter Optimization of Integral Rolled Spiral Finned Tube Bundle Heat Exchangers, *Processes, 11* (2023), 2192
[8] Zhang, D., *et al*., Experimental Study on Heat Transfer and Flow Resistance Characteristics of Integral Rolled Spiral Finned Tube Bundles Heat Exchangers, *Case Studies in Thermal Engineering, 52* (2023), 2192
[9] Kang, H. J., *et al*., Experimental Study on Heat Transfer and Pressure Drop Characteristics of Four Types of Plate Fin-and-Tube Heat Exchanger Surfaces, *Journal of Thermal Science, 3* (1994), Mar., pp. 34-42
[10] Wang, C. C., *et al*., Effect of Waffle Height on the Air-Side Performance of Wavy Fin-and-Tube Heat Exchangers under Dehumidifying Conditions, *Heat Transfer Engineering, 20* (2000), 5, pp. 45-56
[11] Wang, C. C., *et al*., Empirical Correlations for Heat Transfer and Flow Friction Characteristics of Herringbone Wavy Fin-and-Tube Heat Exchangers, *International Journal of Refrigeration, 25* (2002), 5, pp. 673-680
[12] Youn, B., Kim, N. H., An Experimental Investigation on the Airside Performance of Fin-and-Tube Heat Exchangers Having Sinusoidal Wave Fins, *Heat and Mass Transfer, 43* (2006), Dec., pp. 1249-1262
[13] Sadeghianjahromi, A., *et al*., Heat Transfer Enhancement of Wavy Fin-and-Tube Heat Exchangers via Innovative Compound Designs, *International Journal of Thermal Sciences, 149* (2020), 110470
[14] Ouyang, X., Hu, H., Simulation Study on Optimal Structure of Circular Corrugated Finned Tube, *International Journal of Thermal Sciences, 179* (2022), 107622
[15] Song, K., *et al*., Heat Transfer Characteristics of Concave and Convex Curved Vortex Generators in the Channel of Plate Heat Exchanger Under Laminar Flow, *International Journal of Thermal Sciences, 137* (2019), Mar., pp. 215-228
[16] Kataoka, K., *et al*., Heat/Mass Transfer in Taylor Vortex Flow with Constant Axial Flow Rates, *International Journal of Heat and Mass Transfer, 20* (1977), 1, pp. 57-63

[17] Johnson, T, R., Joubert, P, N., The Influence of Vortex Generators on the Drag and Heat Transfer from a Circular Cylinder Normal to an Airstream, *ASME Journal of Heat and Mass Transfer, 90* (1969), 1, pp. 91-99
[18] Wang, Y., *et al*., Numerical Investigation on Air-Side Heat Transfer Enhancement of Wavy Finned Tube Air Cooler for Underground Tunnels, *Applied Thermal Engineering, 269* (2025), 126061
[19] Liu, X., *et al*., Numerical Analysis on Heat Transfer Enhancement of Wavy Fin-Tube Heat Exchangers for Air-Conditioning Applications, *Applied Thermal Engineering, 199* (2021), 117597
[20] Su, M., *et al*., Numerical Design of Efficient Slit Fin Surfaces with Strips in Different Directions, *International Journal of Thermal Sciences, 192* (2023), 108421
[21] Karabacak, R., Yakar, G., Forced Convection Heat Transfer and Pressure Drop for a Horizontal Cylinder with Vertically Attached Imperforate and Perforated Circular Fins, *Energy Conversion and Management, 52* (2011), 8-9, pp. 2785-2793
[22] Song, K., *et al*., Thermal Performance Promotion of a Novel Double-Tube Heat Exchanger by Helical Fin with Perforations, *International Communications in Heat and Mass Transfer, 150* (2023), 07189
[23] Zaidan, M. H., *et al*., Assessment of Heat Transfer and Fluid Flow Characteristics within Finned Flat Tube, *Case Studies in Thermal Engineering, 12* (2018), Sept., pp. 557-562
[24] Wu, J., *et al*., Numerical Analysis of Shell Side Performance of Spiral finned Self-Supporting Heat Exchanger, *Petroleum Refining and Chemical Engineering*, *8* (2007), pp. 66-70
[25] Wu, J., *et al*., Experimental Study on Enhanced Heat Exchange of Spiral Finned Self-Supporting Heat Exchanger, *Thermal Energy and Power Engineering*, *2* (2008), pp. 157-160+215-6
[26] Wu, J., *et al*., Numerical Study on Fluid Flow and Heat Transfer Characteristics in Spiral Wound Heat Exchanger with Helical Rods, *International Communications in Heat and Mass Transfer*, *167* (2025), 109622
[27] Wu, J., *et al*., Numerical Study on Heat Transfer Characteristics of Helically Coiled Grooved Elliptical Tube Heat Exchanger, *International Journal of Heat and Fluid Flow*, *110* (2024), 109624
[28] Guo, Z. Y., *et al*., The Field Synergy (Coordination) Principle and Its Applications in Enhancing Single Phase Convective Heat Transfer, *International Journal of Heat and Mass Transfer*, *48* (2005), 9, pp. 1797-1807
[29] FaJiang, H., *et al*., Experimental Investigation of Heat Transfer and Flowing Resistance for Air Flow Cross over Spiral Finned Tube Heat Exchanger, *Energy Procedia, 17* (2012), Part A, pp. 741-749

Paper submitted: October 29, 2025
Paper revised: December 29, 2025
Paper accepted: January 5, 2026
2026 Published by the Vinča Institute of Nuclear Sciences, Belgrade, Serbia.
This is an open access article distributed under the CC BY 4.0 terms and conditions.